THE JOURNAL OF PHYSICAL CHEMISTRY LETTERS
A JOURNAL OF THE AMERICAN CHEMICAL SOCIETY

pubs.acs.org/JPCL

Letter

Quantum-Classical Simulation of Molecular Motors Driven Only by Light

Atreya Majumdar* and Thomas L. C. Jansen*

Cite This: *J. Phys. Chem. Lett.* 2021, 12, 5512−5518

Read Online

ACCESS | Metrics & More | Article Recommendations | Supporting Information

ABSTRACT: Molecular motors that exhibit controlled unidirectional rotation provide great prospects for many types of applications, including nanorobotics. Existing rotational motors have two key components: photoisomerization around a π-bond followed by a thermally activated helical inversion, the latter being the rate-determining step. We propose an alternative molecular system in which the rotation is caused by the electric coupling of chromophores. This is used to engineer the excited state energy surface and achieve unidirectional rotation using light as the only input and avoid the slow thermally activated step, potentially leading to much faster operational speeds. To test the working principle, we employ quantum-classical calculations to study the dynamics of such a system. We estimate that motors built on this principle should be able to work on a subnanosecond time scale for such a full rotation. We explore the parameter space of our model to guide the design of a molecule that can act as such a motor.

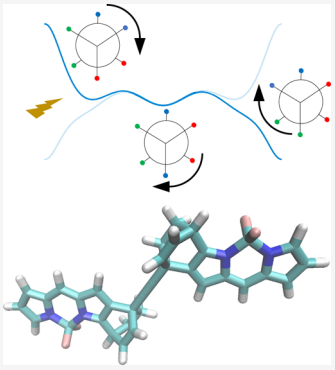

Naturally occurring molecular machines play an important role in various biological pathways that are crucial to life, such as the transport of cellular matter by kinesin protein[1] or facilitating muscular contraction by myosin.[2] The ubiquity of this kind of system in biology has triggered the research in the synthesis of artificial molecular machines in the past few decades.[3] A molecular machine responds to an external stimulus by changing the conformation of a submolecular unit. This change can lead to the molecule functioning as a motor,[4−6] a shuttle,[7] a switch,[8] tweezers,[9] or a propeller.[10] Molecular motors are chiral molecules that exhibit unidirectional rotational motion upon being stimulated. Upon combination of several such motors, even nanocars that can move on surfaces have been synthesized.[11−13] With such useful properties, these motors might pave the way for efficient transport on the nanoscale and could be crucial in novel applications of drug delivery or nanorobotics.[14,15] The aim of this paper is the theoretical study of the feasibility of a new motor design that is driven by only light.

The original light-driven motor[4] relies on four successive steps to achieve a complete unidirectional rotation. In essence, moieties around a π-bond experience conformational changes through this cycle. On the incidence of light and with the proper temperature bath present, the molecule goes through successive *cis*−*trans* isomerization[16] and helical inversion steps to return to the original conformation. The first *trans*−*cis* isomerization occurs by exciting the molecule to the first excited state whereby it relaxes to the next metastable *cis* isomer. Then it awaits a thermalization step after which the helical stacking of the molecule is inverted. Another photoisomerization step follows, which is again succeeded by a thermally assisted helical inversion.[17] The time scale of this rotation is limited by the rate-determining thermalization step. In this step, the system waits in the ground state for a thermal fluctuation to drive it over the potential energy barrier for the helical inversion to occur. Even in the fastest of systems, this makes the half-life of the rotation as slow as 6 μs.[18] On the contrary, the time scale related to the photoisomerization process is on the order of pico-seconds.[16,19] Making the thermally assisted step faster or eliminating it would thus potentially allow for dynamics, that is orders of magnitude faster than the currently existing molecular motors. For the efficiency and overall speed of any light-driven molecular motor, it is of course also crucial that the quantum yield of the light-driven strokes is high.[16,20]

This Letter presents a novel approach for a molecular design in which the thermally assisted barrier crossing step is circumvented and primarily photochemical effects are utilized to drive the full rotation. The new design will have a downhill thermalization step, where the energy applied by the electronic excitation is dissipated to the environment. In particular, the electric coupling between excited states of dye molecules is employed in a dimer system to generate torque on the molecule that drives the rotation. The excited state potential energy surfaces (PESs) can be engineered to facilitate an asymmetric motion of the relevant degree of freedom, the dihedral angle

Received: March 24, 2021
Accepted: May 29, 2021
Published: June 7, 2021

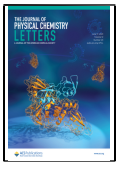

https://doi.org/10.1021/acs.jpclett.1c00951
J. Phys. Chem. Lett. 2021, 12, 5512−5518

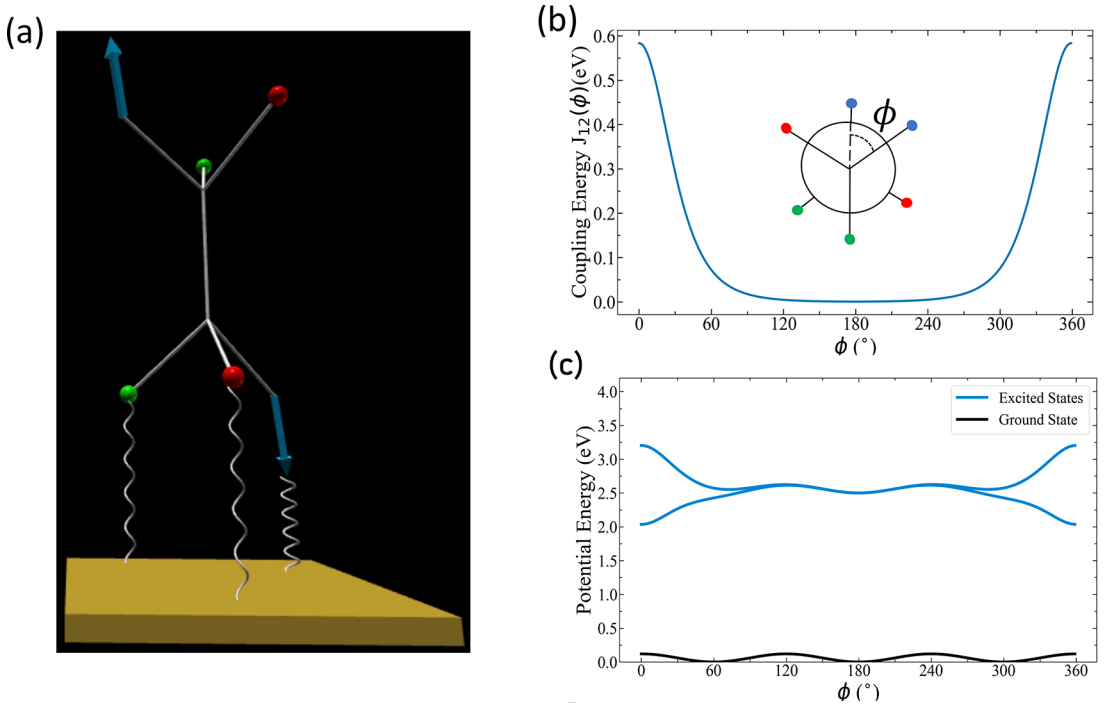

Figure 1. (a) Geometrical schematic of the light-driven motor attached with one end to a surface. One pair of the substituents on either end of the molecule are chromophores illustrated by their transition dipoles (shown as blue arrows). The other substituents (red and green) are chosen in a manner that makes the molecule chiral. (b) The inset shows the Newman projection of the molecule and the angle ϕ, which is the dihedral angle between the two dipoles. The plot shows the variation of the dipole−dipole coupling energy with the dihedral angle. (c) Adiabatic ground and excited state potential energy surfaces. The excited states are split because of dipolar coupling.

between the transition dipole moments of the two chromophore units. An estimate is then made of the time scale at which the molecular motor rotates. Finally, the parameter space of the model is explored to locate the regime in which the motor would potentially function. This understanding guides the future design of a real molecule that can be synthesized and characterized in the laboratory. The strategy is somewhat similar to that used to design other functional materials, and the driving force is the same as found in excimer formation.[21,22] The design presented here is significantly different from those previously proposed for rotary motors driven only by light[23−25] in that, here, the rotation will not be around a double bond.

The monomer units of the system that house the chromophores are connected via a σ-bond or potentially a combination of a σ-bond, a triple bond, and another σ-bond. The other substituents are chosen to make the molecule chiral, thereby stabilizing the ground state potential minimum at the intended initial configuration and ensuring that the molecule has a preferred direction of rotation in the ground state. In the system considered here, one of the monomers is chemically attached to a surface whereas the other end remains free, as depicted schematically in Figure 1a. The degree of freedom of the main interest, the dihedral angle (ϕ) (Figure 1b), is simulated quantum mechanically, and all other degrees of freedom are treated classically as Brownian oscillators. The total Hamiltonian ($\hat{H}(t)$) of the system is the sum of the system Hamiltonian ($\hat{H}_S$)[26,27] and the bath Hamiltonian ($\hat{H}_B(t)$). In the diabatic representation, the Hamiltonian can be expressed as ($\hbar = 1$)

$$\hat{H}_S = \sum_{i=0}^{2}\sum_{j=0}^{2} |i\rangle(\hat{T}\delta_{ij} + \hat{V}_{ij})\langle j| \tag{1}$$

where the ground state is assigned the number 0 and the two states in which one of the chromophores is excited are assigned the numbers 1 and 2. The kinetic energy operator for the rotation is defined

$$\hat{T} = -\frac{1}{2I}\frac{\partial^2}{\partial\phi^2} \tag{2}$$

where I is the moment of inertia for the rotation about angle ϕ. The electric coupling between the two chromophores is

$$\hat{V}_{12} = \hat{V}_{21} = J_{12}(\phi) \tag{3}$$

The coupling between the ground and excited states is set to zero. It is assumed that the ground state PES varies with the dihedral angle (ϕ) as a simple sinusoid having an amplitude of W_0. Moreover, it is assumed that the uncoupled excited state has the same form:

$$\hat{V}_{00} = \hat{V}_{11} = \hat{V}_{22} = \frac{W_0}{2}(1 + \cos 3\phi) - \varepsilon\cos(\phi - 60°) \tag{4}$$

The second term in the PES is a small perturbation ($\varepsilon \ll W_0$) that is introduced to break the symmetry and has a physical origin in the choice of the red and green substituents. This introduces chirality and biases the ground state wave function of the electronic ground PES to a global minimum around $\phi = 60°$. In practice, ε should not be too small compared to k_BT to localize the initial wave function in the initial state, but not so large that it perturbs the dynamics in the excited state. In realistic systems, this should not be difficult to engineer. The values of energy parameters W_0 and ε are listed in Table 3. We here deliberately choose a simple PES to avoid an unreasonable number of free parameters and keep focus on the general

https://doi.org/10.1021/acs.jpclett.1c00951
J. Phys. Chem. Lett. 2021, 12, 5512−5518

principle. If a sufficiently accurate PES can be obtained for a specific candidate molecule, this can of course be used to replace the PES used here to evaluate the efficiency of that specific molecule.

The electric coupling is approximated with the transition dipole coupling model resulting in the following dependence where the transition dipole positions and orientations depend on dihedral angle ϕ:

$$J_{12}(\phi) = \frac{1}{4\pi\varepsilon_0}\left[\frac{\vec{\mu}_1\vec{\mu}_2}{|\vec{r}_{12}|^3} - 3\frac{(\vec{\mu}_1\vec{r}_{12})(\vec{\mu}_2\vec{r}_{12})}{|\vec{r}_{12}|^5}\right] \quad (5)$$

where $\vec{\mu}_1$ and $\vec{\mu}_2$ are the transition dipole moments for the two monomer sites and $\vec{r}_{12}$ is the vector between the two point dipoles. The resulting variation in the electric coupling for the set of parameters chosen for the simulation is depicted in Figure 1b, while the variation in the eigenenergies is shown in Figure 1c. Figure 2 shows the geometrical parameters of our model,

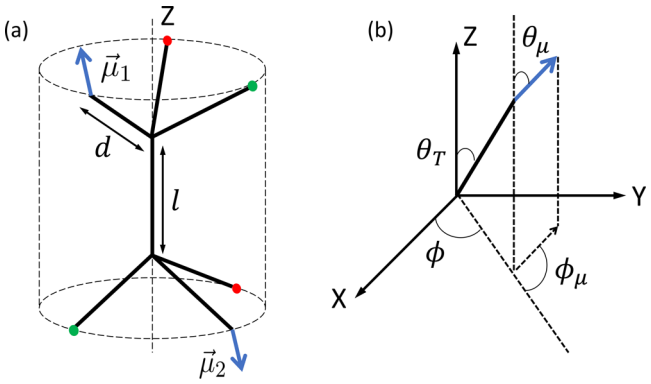

Figure 2. Detailed geometric description of the model. (a) Spatial parameters l and d of the molecule that defines the relative position of the two transition dipole moments $\vec{\mu}_1$ and $\vec{\mu}_2$. (b) Angular parameters θ_μ, ϕ_μ, and ϕ that define the orientation of the transition dipole moments.

including dihedral angle ϕ that is modeled as the azimuthal angle in a cylindrical coordinate system. In Figure 2a, l represents the distance between the two monomer units and d denotes the distance of the point dipole from the end of the bond connecting the monomers. Figure 2b depicts the angular parameters (θ_T, θ_μ, and ϕ_μ) that determine the orientation of the dipole moments and are assumed to be fixed in the rotating frame. Angle θ_T is the tetrahedral angle by which each of the three connecting bonds is titled with respect to the Z axis and the orientation of the dipole is characterized by angular parameters θ_μ and ϕ_μ. Transition dipole moments $\vec{\mu}_1$ and $\vec{\mu}_2$ are of the same magnitude $|\vec{\mu}|$, but points in opposite directions. The dihedral angle (ϕ) is the degree of freedom that is explicitly simulated in this work. The orientations of the transition dipoles for the two chromophores were chosen such that they are almost parallel to the rotation axis ($\theta_\mu = 10°$). This ensures that the upper PES has its maximum dipolar coupling strength at $\phi = 0°$ and provides a non-zero oscillator strength to the upper PES. The values of the aforementioned parameters used in our simulations are summarized in Table 1.

The potential energy part of the Hamiltonian is diagonalized to find the split excited state surfaces, and the obtained electronic ground and first two excited states are shown in Figure 1c in the angular basis. The two excited state PES surfaces have opposite slopes at angular ranges near the initial configuration,

Table 1. Geometrical Parameter Values Used in the Presented Simulations

parameter	value
$\lvert\vec{\mu}\rvert$	8 D
l	0.56 nm
d	0.14 nm
θ_T	70.53°
θ_μ	10°
ϕ_μ	0°
I	36.14 amu nm^2

and consequently, the molecule experiences opposite torques depending on the electronic state. The central idea of this model is to utilize this asymmetry to complete the unidirectional motion. The bath Hamiltonian ($\hat{H}_B$) is modeled to be linearly coupled to a bath degree of freedom $x(t)$ as

$$\hat{H}_B(t) = \sum_{i=1}^{2} |i\rangle\eta x_i(t)\langle i| \quad (6)$$

where η is a proportionality constant that depends on the strength of the coupling between the bath degree of freedom and the environment. The bath degree of freedom $x_i(t)$ for the ith site evolves as a Brownian oscillator and derives the fluctuations from the surface to which it is attached. This degree of freedom, treated classically, evolves according to the Langevin equation of motion:[28]

$$m\ddot{x} + \gamma\dot{x} + kx = F_R(t) \quad (7)$$

A mass of m is associated with the bath coordinate x, and it undergoes a damped harmonic motion under friction, contributed by γ and having a spring constant k. The oscillator is driven by a white random force $F_R(t)$ that follows a Gaussian distribution with a zero mean and a standard deviation of $\sqrt{\frac{2k_BTm\gamma}{\Delta t}}$, where Δt is the time step of the numerical integration, which is employed to solve the differential equation. The second-order Runge−Kutta method was used to integrate the equation over the entire time of the simulation with the initial position and velocities drawn from two Gaussian distributions with means of zero and standard deviations of $\sqrt{\frac{k_BT}{k}}$ and $\sqrt{\frac{k_BT}{m}}$, respectively.[29]

Because in our simulations one end of the molecule is attached to a gold surface, it is assumed that the fluctuations in x are derived from the motion of the gold atoms. With this motivation, parameters m, γ, and k are chosen such that they represent values of the atomic mass, the spread, and the mean of phonon spectra of gold, respectively.[30]

The values of the parameters used for the Brownian oscillator simulation are listed in Table 2.

Table 2. Parameter Values Related to the Classical Brownian Oscillator Simulations

parameter	value
Δt	0.05 fs
m	196.95 amu
γ	3.14 ps^{-1}
k	51.6 nN/nm
η	5.87 eV/nm

https://doi.org/10.1021/acs.jpclett.1c00951
J. Phys. Chem. Lett. 2021, 12, 5512−5518

The $x_i(t)$ term breaks the symmetry between the two chromophores as the immediate bath environments for the two sites are generally different.

The ground state Hamiltonian is diagonalized to find the ground state wave function, which peaks at 60°, because of the chiral perturbation. Given that the spacing between the ground state and the uncoupled first excited state is E_0, the wave function is selectively excited to the higher excited state by shining a laser pulse having a Gaussian energy profile with a mean photon energy of E_{laser} and a width of σ_{laser}. This ensures that the resultant wave function peaks at ∼40° on the upper PES. This angular value is chosen because of the favorable slope at that angle that results in a torque which propels the molecule to rotate. The energy-related values used in the simulation are listed in Table 3.

Table 3. Parameters Related to Energy That Are Used in the Simulations

parameter	value
E_0	2.5 eV
W_0	0.12 eV
ε	0.001 eV
E_{laser}	2.81 eV
σ_{laser}	0.05 eV

The temporal evolution of the wave function is governed by the time-dependent Schrödinger equation:

$$\frac{d\psi(\phi, t)}{dt} = -i\hat{H}(t)\psi(\phi, t) \quad (8)$$

The wave function $\psi(\phi, t)$, following this quantum mechanical equation of motion, is propagated over small time intervals Δt, over which the Hamiltonian is approximately constant, using[31]

$$\psi(\phi, t + \Delta t) = e^{-i\hat{H}(t)\Delta t}\psi(\phi, t) \quad (9)$$

The time interval Δt is chosen such that it is smaller than both the time scale associated with the largest energy difference in the system and the environmental fluctuation correlation time scale. The evolution of the probability densities $[|\psi(\phi, t)|^2]$ corresponding to the two wave functions (light and dark blue) in the site basis is shown in Figure 3a−e for a single bath realization. The initially excited wavepacket starts at 40° and around 50 fs approaches 60° where it encounters a minimum (Figure 3a). It goes over the first barrier with reduced momentum, and a part of it is reflected from the second potential barrier. The small peaks close to 60° in Figure 3b depict this counter-motion of a small part of the wave function. At 900 fs, when most of the wave function is around 300°, the part of the wave function that still resides in the upper PES is reflected from the high barrier. The other part, which has gone on to the lower PES, continues the unidirectional motion as shown in Figure 3c. Figure 3d shows the wave functions at 1.1 ps where a significant part of the wave function has completed the full rotation. At longer times (Figure 3e), the motion of the wave functions becomes incoherent as the time scale of the simulation approaches the time scale of the fluctuations in the system. An estimation of the quantum yield of rotation gives a value of 33%. The calculation details are presented in the section 1 of the Supporting Information. Propagation methods accounting explicitly for thermalization[32−34] may improve the efficiency estimate in the future. The unidirectionality is lost after one rotation. Following this full rotation, the energy supplied by the electronic excitation needs to be dissipated to the environment

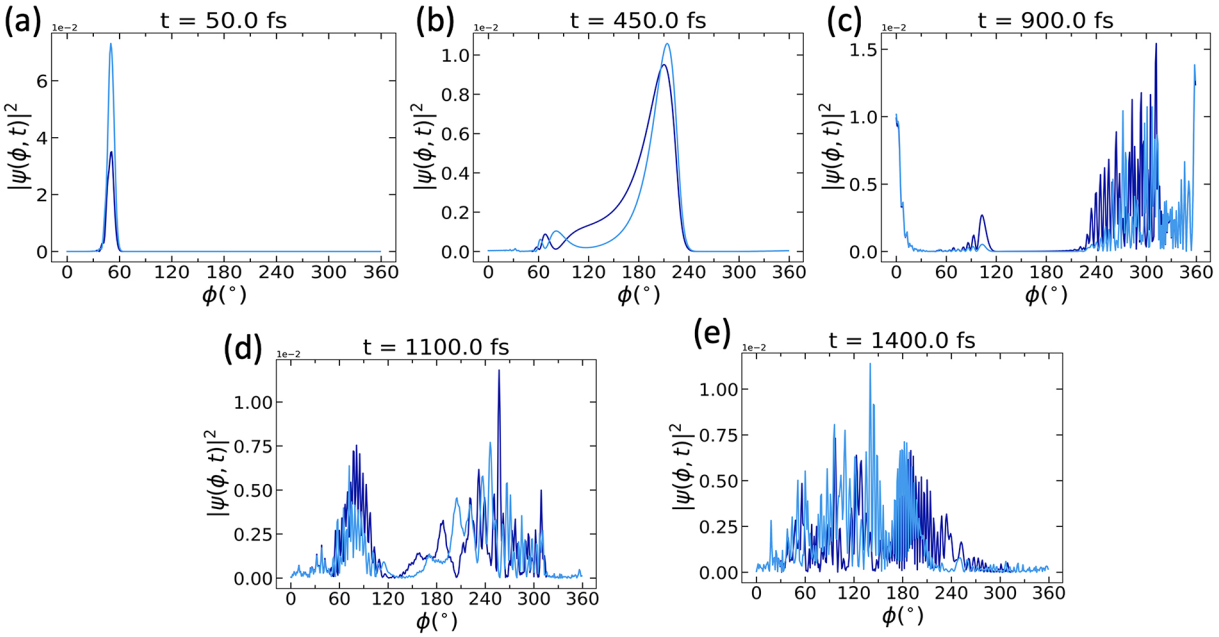

Figure 3. Initially excited probability density propagating according to the time-dependent Schrödinger equation for a single-bath realization. The light and dark blue plots denote the two different sites. There are different stages during the evolution. (a) Initial probability density after propagating for 50 fs upon being excited to the upper excited state potential energy surface. (b) The wave packet has propagated toward larger dihedral angles. Part of the wave was reflected by one of the smaller potential barriers shown in Figure 1 and is smeared over a range toward smaller dihedral angles. (c) A part of the density is reflected, whereas another part is continuing its unidirectional motion. (d) A part of the wave packet has come back to the initial spot near 60°. (e) Subsequent evolution of the probability density.

https://doi.org/10.1021/acs.jpclett.1c00951
J. Phys. Chem. Lett. 2021, 12, 5512−5518

or to a nearby quenching molecule before a new rotation can be induced by a subsequent excitation and a new rotation. As the barriers on the ground state potential surface should be fairly shallow, a breaking mechanism[23] may be employed to prevent random rotation in the ground state, when the motor is not in operation.

To estimate the time at which the complete rotation occurs for a part of the wave function, the probability density at 40° is monitored as a function of time in Figure 4. Because the initial

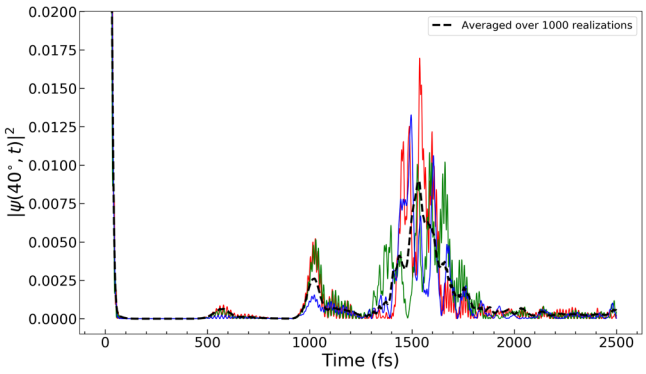

Figure 4. Estimation of the rotation time scale by looking at the probability density at 40°. The density decreases very rapidly as the wave packet moves away and again increases at around 1000 fs when the part of the wave packet that has completed the rotation returns to that angle. The smaller bump at 600 fs is the reflected part of the density that came back. The blue, green, and red lines show three different realizations, while the dotted black line is the evolution of the density averaged over 1000 realizations of the simulation.

laser-excited wave function was around that angle, the density at the beginning is very high. As the wavepacket moves toward larger angles, this value sharply drops. It shows a slight increase at ∼550 fs due to the reflected wavepacket as shown in Figure 3b. The next hump at ∼1000 fs denotes the time at which the rotation has reached completion as shown in panels c and d of Figure 3. The other features around 1400 fs correspond to the incoherent propagation of the wave function where it becomes smeared over the whole angular range.

From the observations in Figures 3 and 4, we can infer that unidirectional motion can be achieved in a time scale of ∼1 ps. The magnitude of the electric coupling determines the splitting between the two states and consequently regulates the propagation of the wave function. In turn, this coupling depends upon the relative distance and orientation of the two transition dipole moments of the dimer molecule. These geometrical parameters should be such that, on one hand, the coupling is close enough to zero so that the bath fluctuations can drive the wave function between the two excited states. On the other hand, the strength of the coupling should be larger than the ground state potential energy barriers to ensure that the excited state PESs are significantly different from the ground state one. With these criteria in mind, the parameter space is explored to find the regime where the design of the molecule makes it likely to act as a motor.

The distance between the two monomer units (l) and the distance of the dipole moment from one end of the unit (d) are identified as two crucial geometric parameters, along with the strength of the dipole moments. Because of the symmetry in our system, coupling energy $J(\phi)$ has its minimum value at 180° and its maximum value at 0°. One criterion that is used is that this minimum value $J(180^\circ) < k_B T$, which means that the coupling attains a sufficiently low value for the thermal fluctuation at temperature T to transfer the wave function between the two PESs. The other condition is that the total change in the coupling, i.e., $J(0^\circ) - J(180^\circ) \geq \frac{W_0}{2}$. In other words, the difference in coupling energy values at different angles is large enough compared to the barriers in the ground state PES. Only when these two conditions are simultaneously satisfied can the molecule have the possibility of acting as a motor. The aforementioned exploration is presented in Figure 5 by a map of the two parameters, l and d, for different values of dipole moment strength μ ($=|\vec{\mu}_1| = |\vec{\mu}_2|$). For a very low dipole moment strength (Figure 5a), the region for which both conditions are satisfied (the green area) is very small and occurs for only small values of both parameters. With the increasing value of the dipole moment, as depicted in Figure 5b−d, this favorable region shifts to cover a larger area in the parameter space that has been explored. This map can be used to screen potential molecules and provide insight into the design of new molecules. The BODIPY molecule is a good chromophore candidate as it has a transition dipole of ∼8 D and a high fluorescence quantum yield, reflecting high stability.[35]

In the simulations presented in this Letter, the ground state and first excited state potentials have been assumed to have the same nuclear component. For screening real molecules, electronic structure calculations have to be carried out to determine the exact shape of the PES. Toward that end, the nature of the bond between the two monomer units would play a crucial role, as well as the substituents present. The moment of inertia considered here was chosen with the BODIPY[35] dye in mind. If retinal molecules were used, the moment of inertia would be 5 times smaller. For molecules with larger sizes and moments of inertia, the dynamics would be slowed. For a realistic system, the assumption of having the other angles (θ_μ and ϕ_μ) fixed has to be relaxed, as well. Finally, a rigorous study of the influence of bath fluctuations on the rotation dynamics would require considering a very specific system and explicitly including the nuclear degrees of the environment. Despite the limitations of the study presented here, the demonstrated basic working principle should apply to real systems and alternative molecular machines can potentially be designed following similar principles; for example, one could design systems that will contract like an artificial muscle using a very similar design principle using pairs of chromophores that attract each other in the excited state. In section 3 of the Supporting Information, we have added the structure and information about a potential candidate molecule. In addition, electronic structure calculations and extensive benchmarking will be required to find a molecule that can also be synthesized and applied in practice. The design proposed here is unlikely to be fully unique. We, for example, foresee that a motor design with more chromophores could be more flexible in design and variations over the essential idea put forward here may be worth exploring in the future.

In summary, in this Letter a new concept of realizing a unidirectional rotary molecular motor using only light has been proposed. A chiral dimer system is shown to undergo unidirectional rotational motion about a dihedral degree of freedom. In a demonstration of the working principle on a model molecule attached to a surface, quantum dynamics revealed a quantum yield of ∼33%. The time scale of such a full rotation is estimated to be on the order of a picosecond for the tested set of parameter values, orders of magnitude faster than existing

https://doi.org/10.1021/acs.jpclett.1c00951
J. Phys. Chem. Lett. 2021, 12, 5512−5518

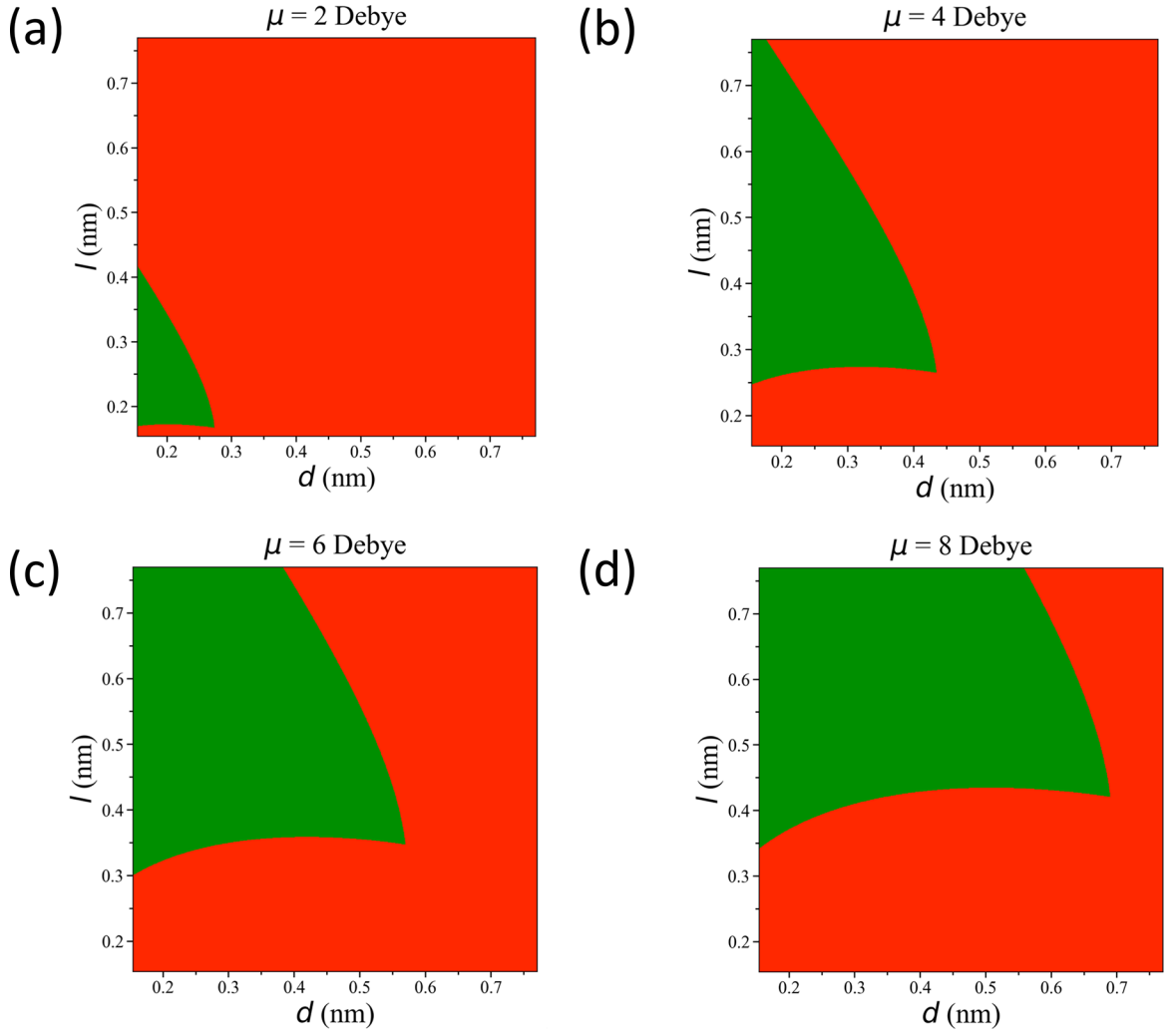

Figure 5. Illustration of the geometric parameter space providing the optimum parameters for the realization of a molecular motor. The green region shows the space for which the two potential energy surfaces cross and the splitting is comparable to the amplitude of potential energy variation as a function of rotation angle ϕ. Panels a–d show the parameter space for different transition dipole moment strengths.

molecular motors. The parameter space was mapped out to find suitable regimes in which a molecule can be designed to act as a molecular motor. Developing, synthesizing, and characterizing a molecule that behaves as predicted here remain important challenges. We foresee that similar design principles may be used for developing molecules with other modes of motion.

■ ASSOCIATED CONTENT

Supporting Information

The Supporting Information is available free of charge at https://pubs.acs.org/doi/10.1021/acs.jpclett.1c00951.

Angular space dynamics movie, momentum space dynamics movie, and candidate motor movie (ZIP)

Calculation of quantum yields, a description of the movies, and a candidate molecule (PDF)

■ AUTHOR INFORMATION

Corresponding Authors

Atreya Majumdar − *University of Groningen, Zernike Institute for Advanced Materials, 9747 AG Groningen, The Netherlands;* Present Address: A.M.: Université Paris-Saclay, CNRS, Centre de Nanosciences et de Nanotechnologies, 91120 Palaiseau, France.; orcid.org/0000-0002-6547-2231; Email: atreyam95@gmail.com

Thomas L. C. Jansen − *University of Groningen, Zernike Institute for Advanced Materials, 9747 AG Groningen, The Netherlands;* orcid.org/0000-0001-6066-6080; Email: t.l.c.jansen@rug.nl

Complete contact information is available at: https://pubs.acs.org/10.1021/acs.jpclett.1c00951

Notes

The authors declare no competing financial interest.

■ ACKNOWLEDGMENTS

Dr. Ana V. Cunha is gratefully acknowledged for helpful discussions about the applied electronic structure calculation method.

■ REFERENCES

(1) Vale, R.; Reese, T.; Sheetz, M. Identification of a Novel Force-Generating Protein, Kinesin, Involved in Microtubule-Based Motility. *Cell* **1985**, *42* (1), 39–50.

(2) Tyska, M. J.; Warshaw, D. M. The Myosin Power Stroke. *Cell Motil. Cytoskeleton* **2002**, *51*, 1–15.

(3) Erbas-Cakmak, S.; Leigh, D. A.; McTernan, C. T.; Nussbaumer, A. L. Artificial Molecular Machines. *Chem. Rev.* **2015**, *115*, 10081−10206.
(4) Koumura, N.; Zijlstra, R. W. J.; van Delden, R. A.; Harada, N.; Feringa, B. L. Light-Driven Monodirectional Molecular Rotor. *Nature* **1999**, *401*, 152−155.
(5) Fletcher, S. P.; Dumur, F.; Pollard, M. M.; Feringa, B. L. A Reversible, Unidirectional Molecular Rotary Motor Driven by Chemical Energy. *Science* **2005**, *310*, 80−82.
(6) Schliwa, M.; Woehlke, G. Molecular Motors. *Nature* **2003**, *422*, 759−765.
(7) Anelli, P. L.; Spencer, N.; Stoddart, J. F. A Molecular Shuttle. *J. Am. Chem. Soc.* **1991**, *113*, 5131−5133.
(8) Feringa, B. L.; van Delden, R. A.; Koumura, N.; Geertsema, E. M. Chiroptical Molecular Switches. *Chem. Rev.* **2000**, *100*, 1789−1816.
(9) Hardouin-Lerouge, M.; Hudhomme, P.; Salle, M. Molecular Clips and Tweezers Hosting Neutral Guests. *Chem. Soc. Rev.* **2011**, *40*, 30−43.
(10) Kelly, T. R.; de Silva, H.; Silva, R. A. Unidirectional Rotary Motion in a Molecular System. *Nature* **1999**, *401*, 150−152.
(11) Morin, J.-F.; Shirai, Y.; Tour, J. M. En Route to a Motorized Nanocar. *Org. Lett.* **2006**, *8*, 1713−1716.
(12) Chiang, P.-T.; Mielke, J.; Godoy, J.; Guerrero, J. M.; Alemany, L. B.; Villagómez, C. J.; Saywell, A.; Grill, L.; Tour, J. M. Toward a Light-Driven Motorized Nanocar: Synthesis and Initial Imaging of Single Molecules. *ACS Nano* **2012**, *6*, 592−597.
(13) Eelkema, R.; Pollard, M. M.; Vicario, J.; Katsonis, N.; Ramon, B. S.; Bastiaansen, C. W. M.; Broer, D. J.; Feringa, B. L. Nanomotor Rotates Microscale Objects. *Nature* **2006**, *440*, 163.
(14) Patel, G. M.; Patel, G. C.; Patel, R. B.; Patel, J. K.; Patel, M. Nanorobot: A Versatile Tool in Nanomedicine. *J. Drug Target.* **2006**, *14*, 63−67.
(15) Wang, J. Can Man-Made Nanomachines Compete with Nature Biomotors. *ACS Nano* **2009**, *3*, 4−9.
(16) Conyard, J.; Addison, K.; Heisler, I. A.; Cnossen, A.; Browne, W. R.; Feringa, B. L.; Meech, S. R. Ultrafast dynamics in the Power Stroke of a Molecular Rotary Motor. *Nat. Chem.* **2012**, *4*, 547−551.
(17) Kazaryan, A.; Kistemaker, J. C. M.; Schäfer, L. V.; Browne, W. R.; Feringa, B. L.; Filatov, M. Understanding the Dynamics Behind the Photoisomerization of a Light-Driven Fluorene Molecular Rotary Motor. *J. Phys. Chem. A* **2010**, *114*, 5058−5067.
(18) Vicario, J.; Walko, M.; Meetsma, A.; Feringa, B. L. Fine Tuning of the Rotary Motion by Structural Modification in Light-Driven Unidirectional Molecular Motors. *J. Am. Chem. Soc.* **2006**, *128*, 5127−5135.
(19) Manathunga, M.; Yang, X.; Orozco-Gonzalez, Y.; Olivucci, M. Impact of Electronic State Mixing on the Photoisomerization Time Scale of the Retinal Chromophore. *J. Phys. Chem. Lett.* **2017**, *8*, 5222−5227.
(20) Conyard, J.; Cnossen, A.; Browne, W. R.; Feringa, B. L.; Meech, S. R. Chemically Optimizing Operational Efficiency of Molecular Rotary Motors. *J. Am. Chem. Soc.* **2014**, *136*, 9692−9700.
(21) Bialas, D.; Kirchner, E.; Röhr, M. I. S.; Würthner, F. Perspectives in Dye Chemistry: A Rational Approach toward Functional Materials by Understanding the Aggregate State. *J. Am. Chem. Soc.* **2021**, *143*, 4500.
(22) Meech, S. R.; Roy, P.; Bressan, G.; Gretton, J.; Cammidge, A. N. Ultrafast Excimer Formation and Solvent Controlled Symmetry Breaking Charge Separation in the Excitonically Coupled Subphthalocyanine Dimer. *Angew. Chem., Int. Ed.* **2021**, *60*, 10568.
(23) García-Iriepa, C.; Marazzi, M.; Zapata, F.; Valentini, A.; Sampedro, D.; Frutos, L. M. Chiral Hydrogen Bond Environment Providing Unidirectional Rotation in Photoactive Molecular Motors. *J. Phys. Chem. Lett.* **2013**, *4*, 1389−1396.
(24) Oruganti, B.; Wang, J.; Durbeej, B. Excited-State Aromaticity Improves Molecular Motors: A Computational Analysis. *Org. Lett.* **2017**, *19*, 4818−4821.
(25) Wang, J.; Oruganti, B.; Durbeej, B. Light-Driven Rotary Molecular Motors without Point Chirality: a Minimal Design. *Phys. Chem. Chem. Phys.* **2017**, *19*, 6952−6956.
(26) Jansen, T. L. C. Simple Quantum Dynamics with Thermalization. *J. Phys. Chem. A* **2018**, *122*, 172−183.
(27) Stock, G.; Woywod, C.; Domcke, W.; Swinney, T.; Hudson, B. S. Resonance Raman spectroscopy of the S1 and S2 states of Pyrazine: Experiment and First Principles Calculation of Spectra. *J. Chem. Phys.* **1995**, *103*, 6851−6860.
(28) Lemons, D. S.; Gythiel, A. Paul Langevin's 1908 paper "On the Theory of Brownian Motion" ["Sur la théorie du Mouvement Brownien," C. R. Acad. Sci. (Paris) 1908 146, 530−533]. *Am. J. Phys.* **1997**, *65*, 1079−1081.
(29) Press, W. H.; Teukolsky, S. A.; Vetterling, W. T.; Flannery, B. P. *Numerical Recipes: The Art of Scientific Computing*, 3rd ed.; Cambridge University Press: New York, 2007.
(30) Lynn, J. W.; Smith, H. G.; Nicklow, R. M. Lattice Dynamics of Gold. *Phys. Rev. B* **1973**, *8*, 3493−3499.
(31) Leforestier, C.; Bisseling, R.; Cerjan, C.; Feit, M.; Friesner, R.; Guldberg, A.; Hammerich, A.; Jolicard, G.; Karrlein, W.; Meyer, H.-D.; et al. A Comparison of Different Propagation Schemes for the Time Dependent Schrödinger Equation. *J. Comput. Phys.* **1991**, *94*, 59−80.
(32) Tully, J. C. Molecular Dynamics with Electronic Transitions. *J. Chem. Phys.* **1990**, *93*, 1061−1071.
(33) Zhou, W.; Mandal, A.; Huo, P. Quasi-Diabatic Scheme for Nonadiabatic On-the-Fly Simulations. *J. Phys. Chem. Lett.* **2019**, *10*, 7062−7070.
(34) Tanimura, Y. Numerically "Exact" Approach to Open Quantum Dynamics: The Hierarchical Equations of Motion (HEOM). *J. Chem. Phys.* **2020**, *153*, 020901.
(35) Loudet, A.; Burgess, K. BODIPY Dyes and Their Derivatives: Syntheses and Spectroscopic Properties. *Chem. Rev.* **2007**, *107*, 4891−4932.

https://doi.org/10.1021/acs.jpclett.1c00951
J. Phys. Chem. Lett. 2021, 12, 5512−5518